NANOCRYSTALLIZATION MECHANISMS OF $Fe_{52}Cr_{18}Mo_7B_{16}C_4Nb_3$ BULK AMORPHOUS STEEL

S. Ahmadi[1] and H. R. Shahverdi[2]

* *Sh.Ahmadi@modares.ac.ir*

Received: March 2013 **Accepted: September 2013**

[1] Biomaterials Group, Materilas and Biomaterials research Center, Tehran, Iran.

[2] Faculty of Engineering, Department of Materials Science, TarbiatModares University, Tehran, Iran.

Abstract: *Crystallization kinetics of $Fe_{52}Cr_{18}Mo_7B_{16}C_4Nb_3$ alloy was evaluated using X-ray diffraction, differential scanning calorimetric (DSC) tests and TEM observations in this research work. In effect, crystallization and growth mechanisms were investigated using DSC tests in four different heating rates (10, 20, 30, 40 K/min) and kinetic models (i.e. Kissinger- Starink, Ozawa, and Matusita methods). Results showed that a two -step crystallization process occurred in the alloy in which α - Fe and Fe_3B phases were crystallized respectively in the structure after heat treatment. Activation energy for the first step of crystallization i.e., α - Fe was measured to be 421 (kj/mol) and 442 (kj/mol) according to both Kissinger- Starink and Ozawa models respectively. Further, Avrami exponent calculated from DSC curves was 1.6 and a two -dimensional diffusion controlled mechanism with decreasing nucleation rate was observed in the alloy. TEM observations reveal that crystalline α – Fe phase nucleated in the structure of the alloy in an average size of 10 nm and completely mottled morphology.*

Keyword: *Bulk Metallic Glasses (BMGs); Bulk Amorphous Alloys (BAAs); Bulk Amorphous Steels (BASs); Structural amorphous steels (SASs); Avrami exponent*

1. INTRODUCTION

Among BMGs and BAAs, bulk amorphous steels (BASs) have been attracted much attention during last decades due to their excellent properties. Ultra- high strength, high hardness (more than 70 HRC), and high corrosion resistance (extraordinary more than 316L stainless steel) are listed among these attractive properties. But, crystallization from amorphous state and formation of nanosize crystals has been named as the most striking feature of the alloys. In fact, unstable structures of bulk amorphous steels can be devitrified to stable nano -structures composed of nanosize crystals and phases by controlled heat treatments above their crystallization temperatures [1-3].

Although there are several of researches devoted to characterization of crystallization kinetics in magnetic classes of bulk amorphous steels, there are only a few attempt about the detailed study of the crystallization behaviors of structural amorphous steels (SASs). In effect, crystallization kinetics of melt- spun $Fe_{83}B_{17}$ and $Fe_{75}Si_9B_{16}$ metallic glass has been investigated with the aid of kinetic models such as Johnson-Mehi- Avrami (JMA) model [4, 5]. In addition, crystallization of α- Fe nano-crystals according a three- dimensional growth model and constant nucleation rate have been suggested during heat treatments of $Fe_{81}B_{13}Si_4C_2$ alloy [6].

In practice, four kinetic models i.e., Kissinger-Starink, Ozawa, Matusita, and Gao-Wang have been widely used to evaluate the kinetics of the crystallization and devitrification in amorphous alloys. All these models are categorized in non-isothermal analysis of crystallization in metallic glasses [7]. In this research, crystallization of α-Fe crystals in a Fe- B- Mo- Cr- C- Nb alloy during annealing process was evaluated for the first time by DSC and XRD tests and also TEM observations. Indeed, crystallization kinetics and growth mechanisms were determined by accomplishing differential scanning calorimetric tests in different heating rates.

2. EXPERIMENTAL PROCEDURES

Multi- component Fe- based alloy ingots were prepared in an arc furnace with nominal compositions of $Fe_{52}Cr_{18}Mo_7B_{16}C_4Nb_3$. Pure iron (99.7 mass %), chromium (99.9 mass %), niobium (99.9 mass %), molybdenum (99.9 mass %), and crystalline B (99.5 mass %) were used to

produce ingots in a rod form. To achieve fully amorphous structures, rapidly solidified thin ribbons with a thickness of about 60 μm were prepared by melt- spinning technique (wheel speed: 32 m/s). Then, amorphous ribbons were annealed under vacuum (10-3torr) in a furnace above the crystallization temperature. X- ray diffraction (XRD) with Cu Kα radiation and differential scanning calorimetry (DSC) at four different heating rates were used to determine the precipitated phases and transformation temperatures. Composition of the ribbons was verified by using energy- dispersive X-ray spectroscopy. A 200 kV JEOL transmission electron microscope equipped with an energy dispersive X-ray spectrometer (INCA PentaFETx3 - Oxford instruments) was used to microstructural evaluations (i.e., TEM observations).

3. RESULTS AND DISCUSSION

3.1. Activation Energy of α - Fe Crystallization

In figure 1, XRD pattern of $Fe_{52}Cr_{18}Mo_7B_{16}C_4Nb_3$ alloy in amorphous state is shown. As can be seen clearly, there is no significant crystalline sharp peak in the chart indicating an amorphous structure. It is mentioned that tiny sharp peaks are related to sort rang order zones (SRO).

The amorphous steel alloy was scanned in DSC tests at 10, 20, 30, and 40 K/min heating rates. Figure 2 shows the DSC curves in different heating rates for the alloy. Two peaks are

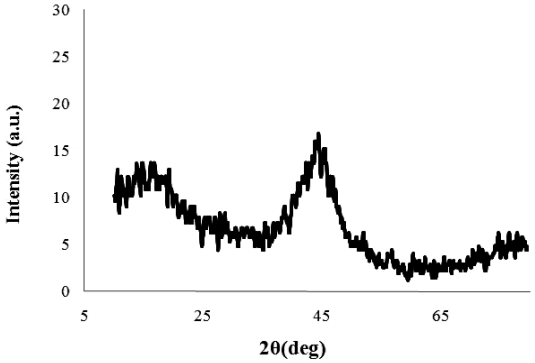

Fig. 1. XRD pattern of the specimen in amorphous state.

Table 1. T_{P1} and T_{P2} for four different heating rates.

Heating Rate	*10 K/min*	*20 K/min*	*30 K/min*	*40 K/min*
T_{P1} (°C)	588	598	603	608
T_{P2} (°C)	710	718	724	730

observed in all thermograms showing two -stage crystallization process in the alloy. Clearly the peak temperatures (T_{P1}, T_{P2}) increase with increasing the heating rate and this suggests that the crystallizations can be classified in the temperature dependent and diffusion controlled processes. In Table1 changes in the first (T_{P1}) and second (T_{P2}) crystallization peaks with increasing heating rate is given.

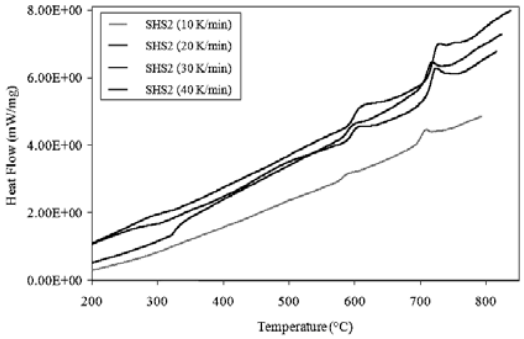

Fig. 2. DSC thermo-grams of the alloy in four different heating rats.

T_o characterize the types of crystallized phases, amorphous ribbons were annealed in two different temperatures. In practice, temperatures were chosen above the first and second

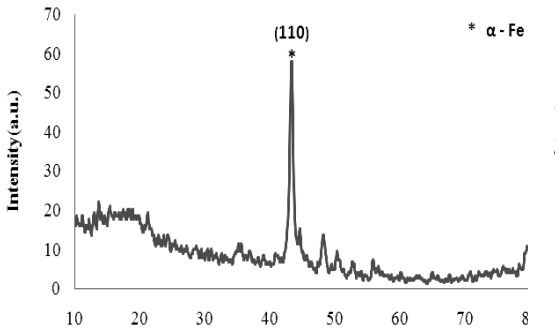

Fig. 3. XRD pattern for specimen annealed at 650°C / 3 hrs.

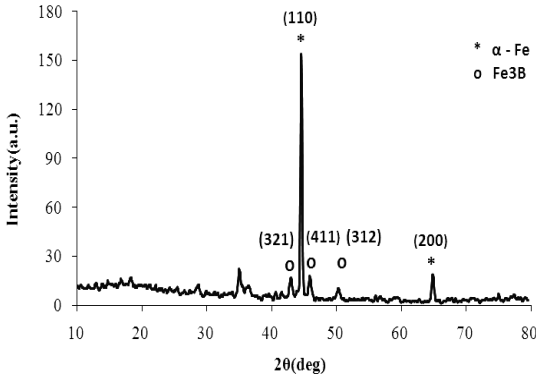

Fig. 4. XRD pattern for specimen annealed at 850°C / 3 hrs.

crystallization peaks i.e., 650°C and 850°C. Figures 3 and 4 show the XRD patterns of crystallized ribbons annealed at temperatures mentioned earlier.

It is clear from the Figures 3 and 4 that α - Fe and Fe_3B phases were crystallized respectively in the structure after annealing process. In general, crystallization of α–Fe, $Fe_{23}C_6$, and Fe_3B phases in 7170 ($Fe_{52.3}Mn_2Cr_{19}Mo_{2.5}W_{1.7}B_{16}C_4Si_{2.5}$) alloy was reported by Branagan [8]. In comparison with the pervious researches, crystallization of $Fe_{23}C_6$ phase was not observed in the alloy; it is thought to be due to insufficient annealing time (3 hrs) in the alloy. In other words, heat treatment at 850°C for 3 hours has no especial effect on the diffusion of carbon in the structure and formation of the $Fe_{23}C_6$ phase. Due to complete crystallization of α – Fe phase after annealing treatment, Kissinger- Starink peak method (equation 1) and Ozawa model (equation 2) were used to investigate the activation energy, Ea, in the first step of crystallization. According to the equation 1, plotting ln (β / T_P^2) versus $1/T_P$ gives a straight line, the slope of it equals to -Ea/R [9].

$$\ln \frac{\beta}{T_P^2} = -\frac{E_a}{RT_P} + C \quad (1$$

Where β is heating rate, R is the gas constant, and T_p is the peak temperature.

Ozawa (equation 2) model was also used to determine the activation energy for the first crystallization peak of the alloy. In this model, plotting ln (β) versus $1/T_P$ gives a straight line and slope of the line equals to -Ea/R.

$$\ln \beta = -\frac{E_a}{RT_P} + C_2 \quad (2$$

Arrhenius plots for the first endothermic heat effect are shown in Figures 5, 6. Activation energy for crystallization of α – Fe phase in the alloy was measured to be 421 (kj/mol) and 442 (kj/mol) according to Kissinger and Ozawa models respectively.

In some other solid state transformation e.g., precipitation hardening and formation of strengthening precipitate in the structure of Al alloys, activation energy required for precipitation was measured to be 120- 135 (kj/mol) [10]. In comparison with precipitation hardening, high value of activation energy in crystallization process of the amorphous alloy can be attributed to mass displacement of atoms.

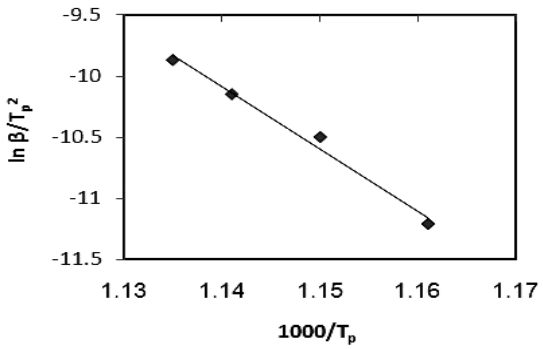

Fig. 5. Arrhenius plot of $\ln(T_P^2/\beta)$ vs $1000/T_P$ for crystallization of α – Fe phase according to Kissinger model.

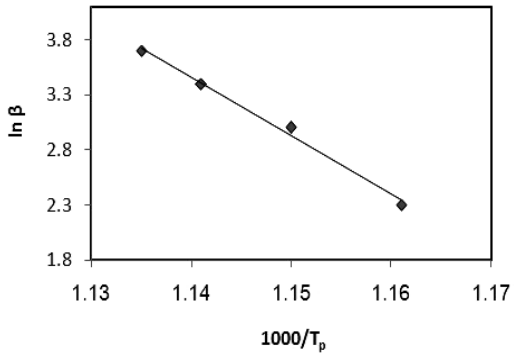

Fig. 6. Arrhenius plot of $\ln(\beta)$ vs $1000/T_P$ for crystallization of α – Fe phase according to Ozawa model.

In other words, activation energy can be spent not only to overcome the energy barrier required to diffusion of atoms but also to nucleation and growth of crystalline phases. In effect, activation energies equal to 355, 370, and 288 (kj/mol) were measured respectively in devitrification of $(Fe_{0.8}Cr_{0.2})_{73}Mo_2W_2B_{16}C_4Si_1Mn_2$, $Fe_{54.5}Mn_2Cr_{15}Mo_2W_{1.5}B_{16}C_4Si_5$, and $Fe_{52.3}Mn_2Cr_{19}Mo_{2.5}W_{1.7}B_{16}C_4Si_{2.5}$ alloys [11]. Thus, it can be said that activation energy for the first step of crystallization in the amorphous steel was considerably increased by alloying with Nb.

3.2. Mechanism of α – Fe Crystallization

To indicate the exact mechanisms of growth in the alloy, Matusita model was used (equation 3).

$$\ln[-\ln(1-\alpha)] = -n\ln(\beta) - 1.052\,(mE_a / RT) + \text{constant} \quad (3$$

Where α is the volume fraction of crystallization, β is heating rate, Ea activation energy, n is Avrami exponent , m is dimensionality of growth, and R is the gas constant. In this research, by plotting ln [-ln (1-α)] versus ln β at constant temperature Avrami exponent was estimated. Furthermore, by plotting ln [-ln (1-α)] versus temperature (T) at constant heating rate (β) dimensionality growth guideline (m) was derived. In figures 7 and 8 variation of ln [-ln (1-α)] versus ln β at constant temperature and variation of ln [-ln (1-α)] versus temperature (T) at constant heating rate (β) are shown respectively.

Matusita model differs with Kissinger- Starink method in that it provides useful information about the Avrami exponent and dimension of growth in devitrification of amorphous alloys. In fact, besides activation energy, mechanisms of growth can be investigated using this method. In general, Avrami exponent (*n*) can be estimated according to equation 4 [9].

$$n = b + pm \quad (4$$

Where n is Avrami exponent, m is dimensionality growth parameter, b is a parameter showing nucleation rate, and p is a parameter showing type of transformation e.g., diffusion controlled transformations. In table 2 explanations of these parameters are given. The amount of Avrami exponent (n) in this research was calculated to be 1.6 by considering the slop of the straight line in fig. 7.

In effect, the average of dimensionality growth parameter (m= 2) can be implied from the slops of straight lines in Fig. 8. Indeed, it is though that devitrification process in $Fe_{52}Cr_{18}Mo_7B_{16}C_4Nb_3$ was carried out by a bulk crystallization mechanism in two dimensions. As mentioned earlier, diffusion controlled crystallization process accomplished in the alloy and thus, the amount of p was considered equal to 0.5. In addition, it is also hypothesized decreasing nucleation rate (b) in crystallization of α–Fe phase during annealing of $Fe_{52}Cr_{18}Mo_7B_{16}C_4Nb_3$

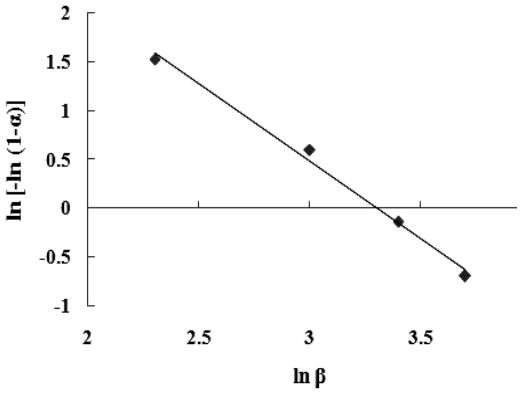

Fig. 7. Ln [-ln (1-α)] as a function of heating rate in constant temperature (T=610°C).

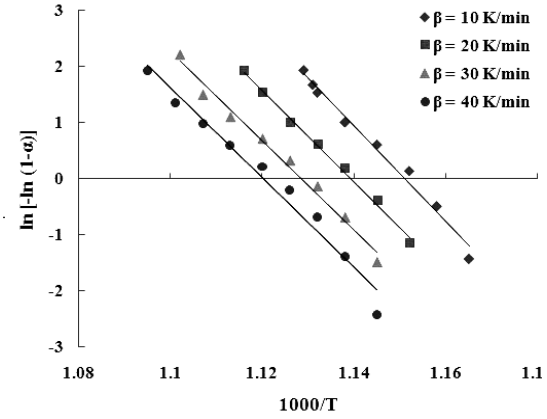

Fig. 8. Matusita plots at different temperatures and constant heating rate.

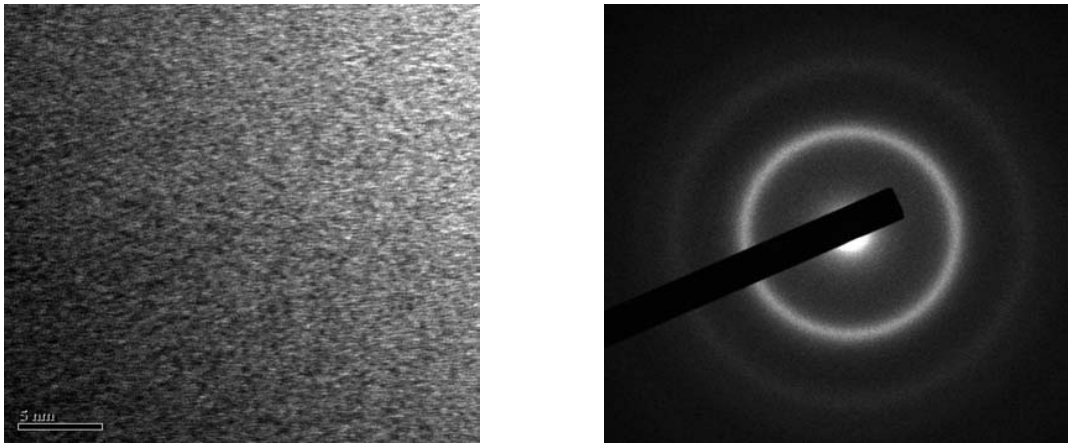

Fig. 9. Microstructure of the alloy in amorphous state.

alloy resulting from equation 4 and the amounts of n, m, and p.

3. 3. Microstructural Observations

In figure 9 microstructure of the primary alloy in amorphous state is shown. Specifically, no crystalline phases are detected in the figure. One of the most striking features of the bulk nanostructured Fe based alloys produced by annealing a preliminary amorphous state is the distinct appearance / morphology of the crystalline phases (i.e. α – Fe, $Fe_{23}C_6$ and $Fe_{23}C_6$). For example, α - Fe and $Fe_{23}C_6$ phases crystallize in the structure of the alloys in mottled and featureless smooth morphologies respectively [14].

In fig. 10 microstructure of the crystalline alloy after heat treatment at 830 °C is shown. It is clear from the images that crystalline α – Fe was nucleate in the amorphous structure after annealing process. Indeed, complex or partially crystalline structure formed due to heat treatment above the first crystalline temperature.

Size and morphology of α – Fe crystalline phases are showed in fig. 11. As mentioned earlier, unique feature of the crystalline phases in structure of the nanostructure Fe base alloys can be effectively used toward the identification of these nanosize phases. It is clearly seen in fig. 11, crystalline α – Fe phase nucleated in the structure an average size of 10 nm and completely mottled morphology.

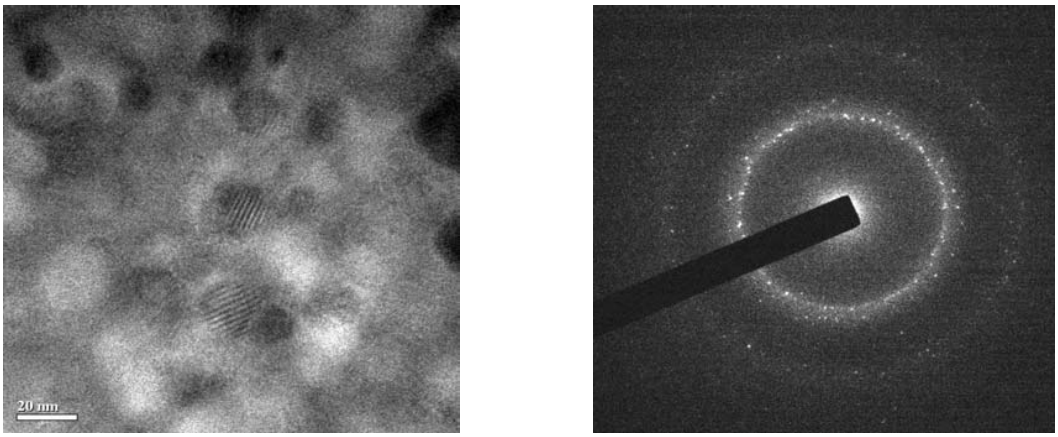

Fig. 10. Microstructure of the alloy in crystalline state.

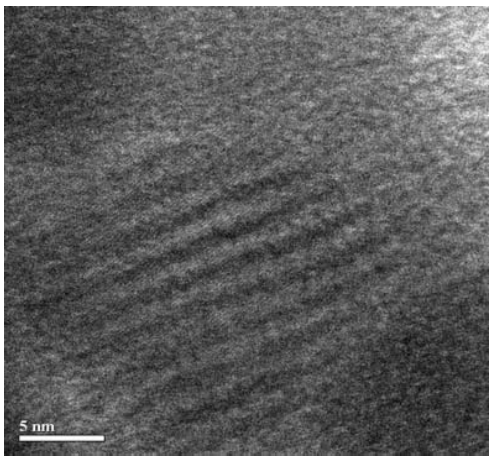

Fig. 11. Crystalline α – Fe phase into the amorphous structure.

Table 2. Explanation of nucleation and growth parameters [6, 13]

Parameter	*Amount*	*Explanation*
m	1	One- dimensional growth mechanism
	2	Two- dimensional growth mechanism
	3	Three- dimensional growth mechanism
p	1	Linear growth (interfacial control)
	0.5	Parabolic growth (diffusion control)
b	>1	Increasing nucleation rate
	0	No nucleation during crystallization (this means that all nuclei may be present before devitrification)
	<1	Decreasing nucleation rate

4. CONCLUSIONS

1. A two- step crystallization process was observed in $Fe_{52}Cr_{18}Mo_7B_{16}C_4Nb_3$ alloy in which α - Fe and Fe3B phases were crystallized respectively in the structure after annealing process.
2. Activation energy for the crystallization of the phase α - Fe was measured to be 421 (kj/mol) and 442 (kj/mol) according to Kissinger- Starink and Ozawa models respectively. It is found that activation energy for the first step of crystallization in the amorphous steel was considerably increased by alloying with Nb.
3. Avrami exponent was measured to be 1.6 in the first step of crystallization of $Fe_{52}Cr_{18}Mo_7B_{16}C_4Nb_3$ alloy.
4. A two -dimensional diffusion controlled growth mechanism and decreasing nucleation rate was found in $Fe_{52}Cr_{18}Mo_7B_{16}C_4Nb_3$ alloy.
5. Crystalline α – Fe phase nucleated in the structure of heat treated $Fe_{52}Cr_{18}Mo_7B_{16}C_4Nb_3$ alloy in an average size of 10 nm and completely mottled morphology.

ACKNOWLEDGMENT

The authors are grateful to Ms. Mohamadinasab (Iranian Minister Processing Research Center) for kindly help toward accomplishing DSC tests.

REFERENCES

1. Wang, W. H., Dong, C., Shek, C. H., "Bulk Metallic Glass",Materials Science and Engineering Reports, 44, 2005, 45.
2. Schroers, J., " The Supper Plastic Forming of Bulk Metallic Glass", JOM, May, 2005, 35-39.
3. Greer, A. L., "Metallic Glass on the Threshold", Materials-today, Vol.12, Jan-Feb., 2009, 14.
4. Solima, A. A., Al-Heniti, S., Al-Hajry, A., Al-Assiri, M., "Crystallization kinetics of melt-spun Fe83B17 metallic glass ", Thermochim. Acta, 413, 2004, 57-62.
5. Chrissafi, K., Maragakis, M. I., K. G., Efthimiadis, Polychroniadis, E. K.," Detailed study of the crystallization behaviour of the metallic glass Fe75Si9B16", J. Alloys Compd. 386, 2005, 165-173.
6. Minic, D. M., Maricic, A., Adnadevic, B., " Crystallization of α-Fe phase in amorphous Fe81B13Si4C2 alloy", J. Alloys Compd. 473, 2009, 363-367.
7. Jain, R., Saxena, N. S., Bhandari, D., Sharma, S. K., " Crystallization kinetics of Cu*x*Ti100−*x* (*x*=43, 50 and 53) glasses", Physica B, 301, 2001, 341-345.
8. Branagan, D. J., "High toughness high hardness iron based PTAW weld materials ", J. Mater. Sci. Eng. A, 428, 2006, 116-123.
9. Starink, M. J., " Analysis of aluminium based alloys by calorimetry: quantitative analysis of reactions and reaction kinetics ", J. Int. Mater. Rev., 49, 2004, 191-226.
10. Ahmadi, S., Arabi, H., Shokuhfar, A., "Formation mechanisms of precipitates in an Al–Cu–Li–Zr alloy and their effects on strength and electrical resistance of the alloy ", J. Alloys Compd. 484, 2009, 90–94.
11. Farmer, J. C., and et al, "High-performance corrosion-resistant materials: iron-based amorphous-metal thermal-spray coatings, high-performance corrosion-resistant materials", UCRL-TR-234787 SAM HPCRM program, FY04 annual report, 2004.
12. Pratap, A., Lad, K., Rao, T., Majmudar, P., Saxena, N. S., "Kinetics of crystallization of amorphous Cu50Ti50 alloy ", J. Non- Crys. Solids, 345 & 346, 2004, 178- 181.
13. Rho, I. C., Yoon, C. S., Kim, C. K., Byun, T. Y., Hong, K. S., "Crystallization of amorphous alloy Co68Fe4Cr4Si13B11 ", J. Mater. Sci. Eng. B, 96, 2002, 48-52.
14. Branagan, D. J., and Tang, Y., " Developing extreme hardness (> 15GPa) in iron based nano-composites<http://www.sciencedirect.com/science/article/pii/S1359835 X02000283>", Appl. Sci. Manu., 33, 2002, 855-859.